Research Article Vol. 3, No. 8 / August 2016 / Optica 809

Lasing in blood

YU-CHENG CHEN, QIUSHU CHEN, AND XUDONG FAN*

Department of Biomedical Engineering, University of Michigan, Ann Arbor, 1101 Beal Ave., Ann Arbor, Michigan 48109, USA
**Corresponding author: xsfan@umich.edu*

Received 23 May 2016; revised 22 June 2016; accepted 23 June 2016 (Doc. ID 266828); published 21 July 2016

Indocyanine green (ICG) is the *only* near-infrared dye approved by the U.S. Food and Drug Administration for clinical use. When injected in blood, ICG binds primarily to plasma proteins and lipoproteins, resulting in enhanced fluorescence. Recently, the optofluidic laser has emerged as a novel tool in bio-analysis. Laser emission has advantages over fluorescence in signal amplification, narrow linewidth, and strong intensity, leading to orders of magnitude increase in detection sensitivity and imaging contrast. Here we successfully demonstrate, to the best of our knowledge, the first ICG lasing in human serum and whole blood with the clinical ICG concentrations and the pump intensity far below the clinically permissible level. Furthermore, we systematically study ICG laser emission within each major serological component (albumins, globulins, and lipoproteins) and reveal the critical elements and conditions responsible for lasing. Our work marks a critical step toward eventual clinical and biomedical applications of optofluidic lasers using FDA approved fluorophores, which may complement or even supersede conventional fluorescence-based sensing and imaging.

OCIS codes: (140.2050) Dye lasers; (140.4780) Optical resonators; (170.6280) Spectroscopy, fluorescence and luminescence; (170.0170) Medical optics and biotechnology; (170.1610) Clinical applications; (170.1470) Blood or tissue constituent monitoring.

http://dx.doi.org/10.1364/OPTICA.3.000809

1. INTRODUCTION

Indocyanine green (ICG) is the *only* near-infrared dye approved by the U.S. Food and Drug Administration (FDA) for clinical use [1,2], such as hepatobiliary surgery [3], sentinel lymph node biopsy [4], and assessment of surgical tumor resection margins [1,5]. ICG has low toxicity and exhibits absorption and emission maxima around 730 and 800 nm (Fig. S1)—both wavelengths are within the ideal spectral window of human tissues for clinical imaging. When injected in blood, ICG binds primarily to plasma proteins and lipoproteins [Fig. 1(a)], resulting in enhanced fluorescence [1,6–9]. In practice, ICG is injected in the blood circulation within the normal clinical dosage range to locate the tumor site and its margin by the higher fluorescence above the background since more blood vessels are grown within/around the tumor site [10,11]. In addition, ICG has been extensively used in *in vitro* preclinical studies of cell lines or animal tissues [8,11–13] with an aim to develop innovative technologies and methodologies for potential clinical applications. In cancer surgery, one of the main prognostic factors for survival rate is complete tumor resection and imaging modalities that allow the specific differentiation and identification of vital structures, which would be of huge benefit during image guided surgery. However, in clinical applications, due to background fluorescence and omnipresent tissue scattering, it remains challenging to obtain high contrast in ICG emission between the tumor and normal tissue for precise tumor detection and margins of excision [12,14–16]. In *in vitro* applications, ICG emission is often not sensitive enough to detect or monitor subtle changes in concentrations or structures in biomolecules, cells, and tissues. Therefore, ICG emission with a superior signal-to-background ratio (SBR) is highly desirable.

Recently, the optofluidic laser has been explored in bioanalysis at the molecular [17–23] and cellular level [21,24–26], in which laser emission, rather than spontaneous emission (i.e., fluorescence), is used as the sensing signal. Laser emission has distinct advantages over fluorescence. First, it is significantly more sensitive to biomolecular and cellular changes than fluorescence [18,19,21,22,27], thanks to the optical feedback in lasing. Second, the laser signal is orders of magnitude stronger and has much narrower linewidth (so that the broadband background can be spectrally filtered out). Finally, due to the threshold behavior in lasing emission, a large contrast (10^2–10^3 fold) can be obtained between before and after lasing [17,28]. All of those result in unprecedented SBR in imaging for tumor localization and sensitivity in *in vitro* biosensing. Therefore, using ICG laser emission could lead to a paradigm change in clinical practice and theranostics. However, while a plethora of previous work has shown the great promise of optofluidic lasers in *in vitro* biomolecular and cellular analysis [17,18,21,22,24,25,27–29], no research has been conducted on the feasibility of laser emission from an FDA approved dye in whole human blood (which is tissue), particularly at the clinically acceptable dye concentration and external pump intensity.

In this article, we carried out for the first time, to the best of our knowledge, a systematic investigation on ICG lasing. We started with each major serological component (albumins,

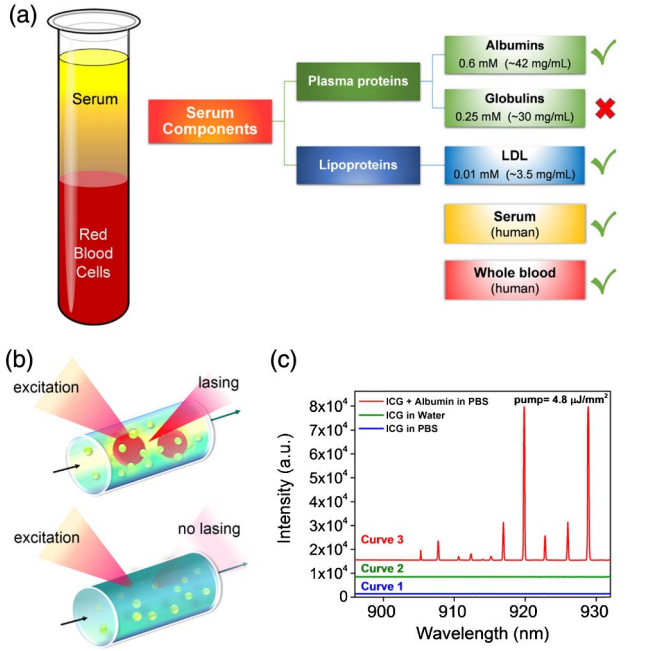

Fig. 1. (a) Schematic diagram showing the composition of blood. The diagram in the rightmost column lists the serological components along with their respective typical concentrations in serum, which we have investigated in the current work. Green checks denote that lasing was achieved with those components when indocyanine green (ICG) within the clinically acceptable concentration range was added, whereas the red cross denotes the component that no lasing was observed from ICG. In addition to testing with serological components, lasing from ICG (within the clinically acceptable concentration range) was observed when it was added to serum and whole blood. (b) Schematic of the ICG laser using a high *Q*-factor optofluidic ring resonator (OFRR). It also illustrates that ICG lasing can only be achieved when ICG binds to serological components such as albumin and lipoprotein. The green circles denote ICG molecules, whereas the red circles denote serological components. During the experiment, ICG was excited by a pulsed optical parametric oscillator (OPO) (pulsewidth, 5 ns; wavelength, 660 nm). (c) Comparison among various emission spectra of ICG. Curve 1, ICG alone in PBS; Curve 2, ICG alone in DI water; Curve 3, ICG with albumin (BSA) in PBS. All curves were obtained under the same pump energy density of 4.8 μJ/mm^2 with the same ICG concentration of 0.4 mM. Curves are vertically shifted for clarity.

globulins, and lipoproteins) to elucidate the critical elements and conditions responsible for ICG lasing. Then, we demonstrated ICG lasing in human serum. Finally, we studied ICG lasing in human whole blood. All the ICG concentrations in serological component studies were well below the commonly used level in *in vitro* biological studies (~1 mM) [29–31] with the lasing threshold on the order of 1 μJ/mm^2. More significantly, lasing could be achieved in human serum and whole blood using ICG within the normal range of clinical dosage (0.01–0.07 mM in human blood [32,33]). The threshold of laser emission in whole blood was 10 μJ/mm^2, 20 times lower than the laser exposure limit for tissues (~200 μJ/mm^2) [34]. At the end of the article, we will present a few possible clinical, preclinical, and biomedical opportunities where the ICG laser may help improve the existing practices and also discuss the challenges that it faces, in particular for *in vivo* clinical applications where the current high-Q cavities may not be applicable.

2. ICG LASING WITH SEROLOGICAL COMPONENTS

Throughout the experiments, we used the optofluidic ring resonator (OFRR) based on a thin-walled fused silica capillary, as illustrated in Fig. 1(b). The circular cross section of the capillary forms the ring resonator that supports the high-Q (>10^7) whispering gallery modes (WGMs). The liquid was injected into the OFRR, in which the evanescent field of the WGM present inside the capillary interacts with the gain medium in the liquid and provides the optical feedback for lasing. See Section 5.

First, as a control experiment, Curves 1 and 2 in Fig. 1(c) show no laser emission from ICG (0.4 mM) alone in either phosphate buffered saline (PBS) or deionized (DI) water at the excitation of 4.8 μJ/mm^2. In fact, no laser emission was observed even when the excitation was as high as 25 μJ/mm^2. This is due to the extremely low quantum yield (0.48%) of ICG in PBS or water. In contrast, in the presence of proteins, rapid binding to ICG results in a significant increase in quantum yield (~4.0%, Fig. S2). Although such a quantum yield is still quite low in comparison with that for many other dyes (such as Rhodamine 6G, Cy3, and Cy5), it is sufficient to support laser emission. In turn, since laser emission is stimulated emission, which is much faster than many nonradiative recombination processes, the quantum yield becomes significantly enhanced once the lasing threshold is achieved. Curve 3 in Fig. 1(c) displays, to the best of our knowledge, the first demonstration of ICG lasing with bovine serum albumin (BSA, 1.2 mM) in PBS under the same excitation as Curves 1 and 2. Strong laser emission peaks emerge on the red side of the ICG fluorescence spectrum (900–935 nm). The linewidth of each peak is approximately 0.18 nm, limited by the resolution of the spectrometer. Those lasing peaks exhibit an SBR as high as 800, nearly 20-fold improvement over that obtained with the fluorescence-based measurement with the same BSA–ICG mixture under the same excitation (Fig. S2 shows a SBR of 40 for ICG–BSA fluorescence versus background), attesting to the advantage of using laser emission in accurate determination of tumor boundaries and sensitive measurement of analyte concentration changes [22].

In order to comprehensively understand the ICG lasing for prospective clinical and preclinical applications, we first studied the ICG lasing behavior of albumin, globulin, and lipoprotein [Fig. 1(a)] with the ICG concentration well below the commonly used level in *in vitro* biological studies [30].

A. Albumins

As presented in Fig. 2, we investigated the ICG laser under different albumin/ICG molar ratios [Figs. 2(a)–2(c)] and various ICG concentrations [Figs. 2(d)–2(g)]. Bovine serum albumin (BSA) in PBS was used as our model albumin, since it is the most abundant protein in blood plasma. We used five solutions with the molar ratio of BSA:ICG ranging from 2:1 to 3.3:1 while fixing the ICG concentration (0.4 mM). Figure 2(a) presents the lasing spectra for different BSA/ICG molar ratios under the same excitation. Detailed studies reveal that different BSA/ICG ratios resulted in different lasing thresholds, as shown in Figs. 2(b) and 2(c), with a minimal lasing threshold of 0.38 μJ/mm^2 for a molar ratio around 3:1. This phenomenon suggests that the ICG binding efficiency (or activation efficiency) plays an important role in ICG lasing. Indeed, in Fig. S3 we carried out regular fluorescence measurement with various BSA/ICG ratios. At a low BSA/ICG ratio,

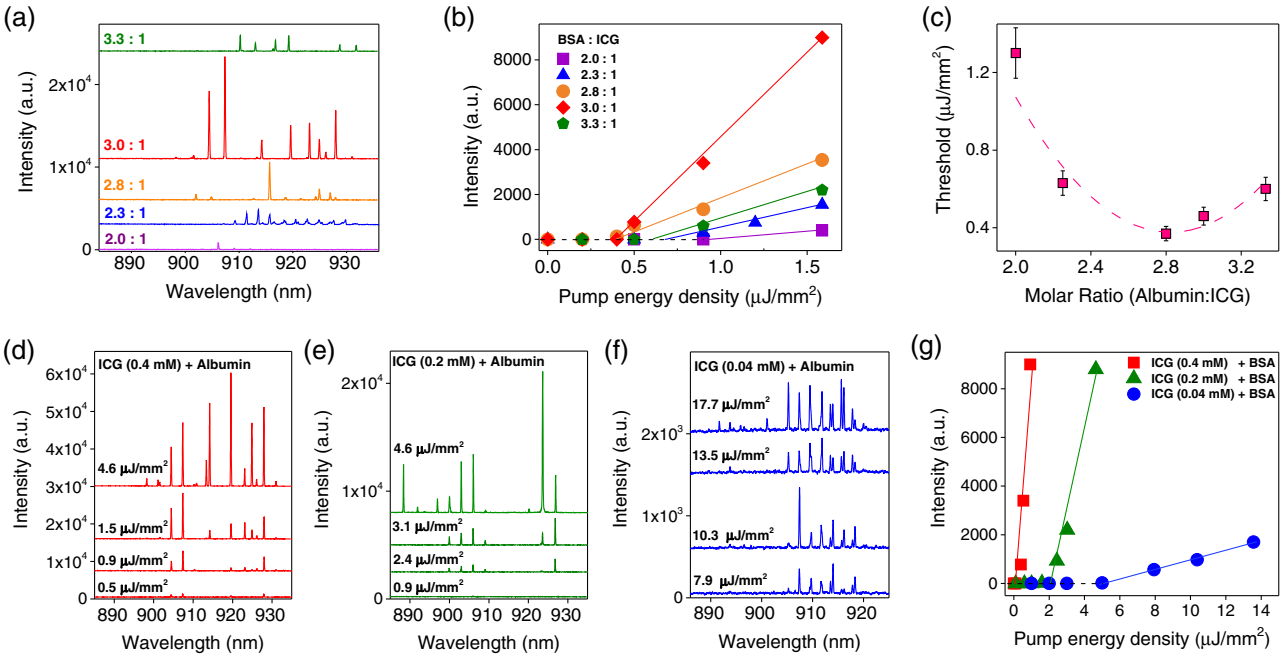

Fig. 2. (a) Lasing spectra of ICG bound to albumin (BSA) with different molar ratios (BSA:ICG varying from 2:1 to 3.3:1). All curves were obtained at the same concentration of ICG (0.4 mM) and the same pump energy density of 1.4 μJ/mm^2. Curves are vertically shifted for clarity. (b) Spectrally integrated (900–930 nm) laser output as a function of pump energy density extracted from the spectra in (a). The solid lines represent the linear fit above the lasing threshold. (c) Lasing threshold as a function of the BSA:ICG molar ratio extracted from the linear fit in (b). The minimum threshold of 0.38 μJ/mm^2 was observed around 3:1. The dashed curve is a quadratic fit to guide an eye. (d)–(f) Lasing spectra of (d) 0.4 mM ICG, (e) 0.2 mM ICG, and (f) 0.04 mM ICG bound to BSA under various pump energy densities. Multimode lasing with irregular spacing was observed as pump intensity increases. All curves in (d)–(f) were obtained with the same BSA:ICG molar ratio of 3:1. Curves are vertically shifted for clarity. (g) Spectrally integrated (900–930 nm) laser output as a function of pump energy density extracted from the spectra in (d)–(f). The threshold based on the linear fit (solid lines) is approximately 0.4, 2.3, and 5.3 μJ/mm^2, respectively, for 0.4, 0.2, and 0.04 mM of ICG.

the fluorescence is relatively weak, suggesting that not all ICG molecules are activated (i.e., bound to BSA molecule). When BSA/ICG = 3, nearly all ICG molecules are bound to BSA and fluorescence starts to saturate. Our fluorescence results not only correlate well with our laser experiments, but also are consistent with a recent finding that a BSA molecule can bind at most one ICG molecule at a time [35,36]. Note that the slight reduction in fluorescence (and hence increase in the ICG lasing threshold) when an excessive amount of BSA was added may be attributed to the additional absorption and scattering loss from BSA.

To study the concentration dependency of the ICG lasing, Figs. 2(d)–2(f) show the lasing spectra of three ICG concentrations at 0.04, 0.2, and 0.4 mM, respectively, when the BSA/ICG ratio was fixed at 3:1. The corresponding lasing threshold curves are plotted in Fig. 2(g), showing the decreased threshold with the increased ICG concentration, which is typical for an optofluidic laser [37]. Even with the lowest ICG concentration (0.04 mM), the lasing threshold was only 5.3 μJ/mm^2. To mimic human plasma, we replaced BSA with human serum albumin (HSA) (fluorescence spectrum in Fig. S2). Once again, a low lasing threshold of 1.68 μJ/mm^2 was obtained when ICG (0.2 mM) binds to HSA (0.6 mM) (Fig. S4). The slightly lower lasing threshold for HSA than for the BSA counterpart (2.3 μJ/mm^2) is due to the relatively high binding affinity of ICG to HSA [35] (hence the ICG quantum yield) as well as the red-shifted fluorescence (and the gain) spectrum (see Fig. S2).

B. Globulins

Next, we studied globulins (GLBs), which take up nearly 35% of the plasma proteins. We used three different concentrations (0.1, 0.2, and 0.3 mM in saline) of γ-GLB (one type of GLBs in blood) to cover the clinically relevant globulin concentration (~0.25 mM). The ICG concentration was fixed at 0.2 mM. However, no lasing emission could be observed even at a high excitation of 25 μJ/mm^2 (Fig. 3). Given that globulins have been

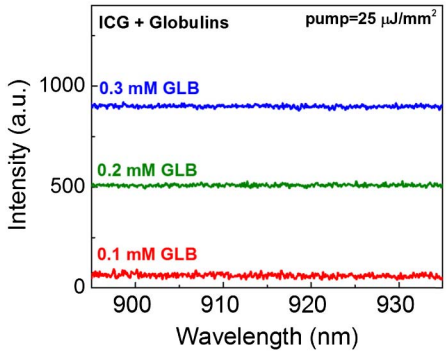

Fig. 3. Emission spectra of the mixture of ICG (0.2 mM) and γ-globulins of different concentrations. All curves were pumped under a pump energy density of 25 μJ/mm^2. In humans, the average concentration of γ-globulins was approximately 0.25 mM, within the concentration range that we investigated in the current work. No lasing was observed. Curves are vertically shifted for clarity.

reported to bind ICG molecules in previous papers [6,38–40], our result is surprising in that GLB is unable to produce lasing. In Fig. S5, we investigated the cause of such negative results and discovered that the quantum yield of ICG when bound to GLB (~0.56%) is not as high as generally thought. It is actually about seven times lower than that of ICG bound to BSA.

C. Lipoproteins

Besides plasma proteins, lipoproteins are another major serological component. Lipoproteins are complex particles that carry lipids such as triglycerides and cholesterol through the bloodstream. They are simply classified into high-density (HDL) and low-density (LDL) lipoproteins, in which the LDL level is regarded as a critical criterion for *cardiovascular* diseases. To determine whether ICG binds to lipoproteins and generates lasing emission, we investigated LDL in PBS with a concentration matching that in human blood (~0.01 mM). The ICG concentration was fixed at 0.2 mM. In Fig. 4(a) we present the lasing emission spectra for LDL pumped under various pump energy densities. Compared to ICG lasing for albumins (center around 920 nm), lasing peaks for LDL emerged at longer wavelengths (around 930 nm) due to the red shift of the ICG–LDL fluorescence (hence the gain) profile (see Fig. S6). Further pump energy density dependent experiments in Fig. 4(b) show a remarkably low threshold of only 0.17 μJ/mm^2, which is more than 10 × lower than the corresponding ICG–BSA lasing [threshold = 2.3 μJ/mm^2 given in Fig. 2(g)] and ICG–HSA lasing (threshold = 1.68 μJ/mm^2 given in Fig. S4), which have the same ICG concentration (0.2 mM). Such a low threshold can be accounted for by the higher gain (proportional to the quantum yield, which is 12.8% for ICG–LDL) of ICG–LDL than that of ICG–BSA and ICG–HSA (see Supplement 1 for discussion).

The above result becomes even more significant when we consider that the LDL concentration (0.01 mM) used was 60 times lower than BSA and HSA (0.6 mM). Previously it was thought that albumins are responsible for enhanced fluorescence in blood [8,38,41]. However, recent studies revealed that ICG might bind mainly to lipoproteins [2,8,36,42,43]. Indeed, our fluorescence measurement shows that lipoproteins bind more ICG and produce approximately three times stronger emission than albumins (Fig. S6), despite a 60 times difference in lipoprotein and albumin concentrations. Our lasing experiment offers another evidence to support the above finding. Furthermore, this suggests that we can obtain ICG lasing for lipoproteins well before for albumins, thus providing a unique means to sensitively monitor lipid levels in blood. In fact, due to the threshold behavior, the signal difference between ICG–lipoprotein (lasing emission) and ICG–albumin (fluorescence) can be as high as 100–1000 times [17,22,28], orders of magnitude larger than the three times difference in the conventional fluorescence measurement.

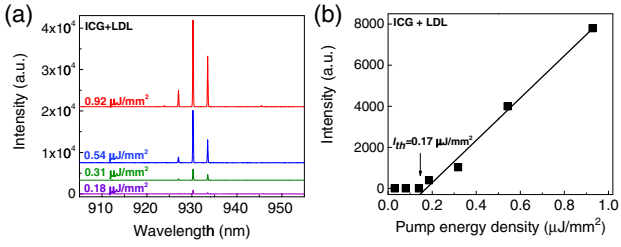

Fig. 4. (a) Lasing spectra of ICG bound to low-density lipoprotein (LDL) under various pump energy densities. The respective concentration of ICG and LDL was 0.2 and 0.01 mM, respectively. Curves are vertically shifted for clarity. (b) Spectrally integrated (920–940 nm) laser output as a function of pump energy density extracted from the lasing spectra. The threshold obtained from the linear fit is approximately 0.17 μJ/mm^2.

D. Serum

Moving a step forward, we explored the ICG lasing possibility in human serum, which contains an abundance of plasma proteins, lipoproteins, antibodies, hormones, and antigens. As a control experiment (Fig. S7), no lasing emission was observed from serum itself. In contrast, as we added ICG (0.2 mM) into serum, lasing emission could easily be observed [Fig. 5(a)]. The lasing threshold is 0.45 μJ/mm^2, falling between that of HSA and LDL, as ICG molecules bind to both plasma proteins and lipoproteins. We also measured serum by using ICG with a concentration as low as 0.04 mM; lasing was obtained with a threshold of 3.4 μJ/mm^2.

3. LASING IN HUMAN WHOLE BLOOD

Our work culminated in achieving direct lasing from "whole blood." As a control experiment, we first flowed human whole blood (2 × diluted in PBS to avoid clogging) through the OFRR as illustrated in Fig. 6(a). Upon excitation, no lasing emission was observed even at a high excitation of 25 μJ/mm^2 (Fig. S8). In contrast, when ICG (0.04 mM) mixed with human whole blood (2 × diluted in PBS to avoid clogging), the lasing band emerged at 915 nm [Fig. 6(b)]. The spectrally integrated laser emission versus pump energy density for blood with ICG is presented in Fig. 6(c), in which the lasing threshold is derived to be approximately 10 μJ/mm^2. The relatively high lasing threshold results from the relatively low concentration of plasma proteins and lipoproteins in whole blood as compared to that in the serum in our previous studies. Moreover, blood cells and other serological components cause disturbance in the gain media, which could significantly degrade the OFRR *Q*-factor. Nevertheless, this lasing threshold is still >20 × lower than the current standard for clinical surgery [34], which is considered to be bio-safe and noninvasive.

Figure 6(d) presents the ICG concentration dependent study of the "blood lasing" under the same pump intensity of 20 μJ/mm^2. The ICG concentration ranged from 0.01 to 0.06 mM, which is within the normal ICG clinical dosage allowed in the circulation system of a human body. Again the blood

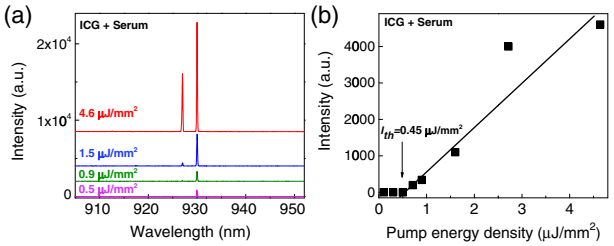

Fig. 5. (a) Lasing spectra of ICG bound to human serum under various pump energy densities. The concentration of ICG was 0.2 mM. Curves are vertically shifted for clarity. (b) Spectrally integrated (920–940 nm) laser output as a function of pump energy density extracted from (a). The threshold obtained from the linear fit is approximately 0.45 μJ/mm^2.

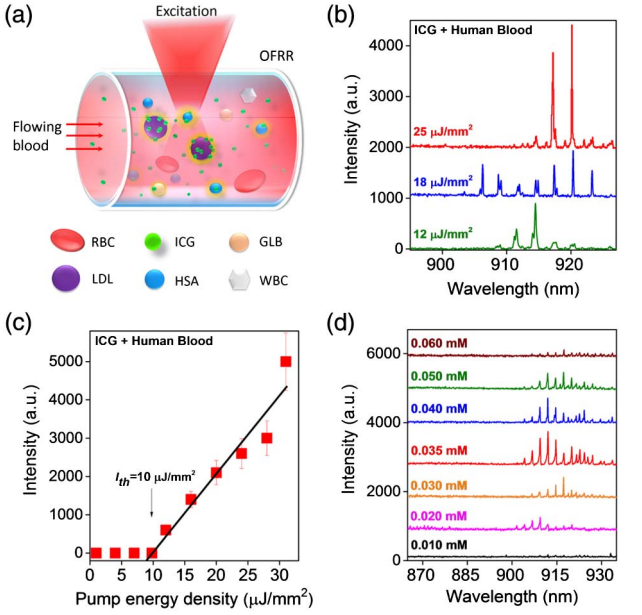

Fig. 6. (a) Schematic showing the excitation process of human whole blood flowing through an OFRR. RBC, red blood cell; WBC, white blood cell (leukocytes). (b) "Blood" lasing spectra under various pump energy densities when ICG (0.04 mM) was injected into the OFRR along with real human whole blood (2 × diluted with PBS buffer to avoid clogging). Curves are vertically shifted for clarity. (c) Spectrally integrated (900–930 nm) laser output as a function of pump energy density extracted from the lasing spectra. (d) Concentration dependent study of the "blood" lasing with various ICG concentrations (0.01–0.06 mM) in human whole blood (2 × dilution with PBS buffer to avoid clogging). A red shift is observed as the pump increases. No lasing emission was observed when the ICG concentration was above 0.06 mM. The pump energy density was fixed at 20 μJ/mm^2. Curves are vertically shifted for clarity.

sample was 2 × diluted. As shown in the black curve of Fig. 6(d), only featureless emission was observed for 0.01 mM ICG. The most prominent blood lasing was achieved when the ICG concentration was around 0.035 to 0.04 mM. However, the laser intensity began to drop dramatically when ICG was higher than 0.06 mM, and no laser emission was observed beyond.

Our concentration dependent laser emission results are consistent with the previous studies on fluorescence, which show that strong fluorescence is observed when the ICG concentration is 0.04 to 0.08 mM [44]. The maximum intensity around 0.065 mM indicates a critical point at which nearly all binding sites in whole blood are occupied by ICG molecules. As such, the fluorescence begins to decrease as the ICG concentration increases beyond 0.065 mM, which can be attributable to two possible factors, i.e., the increased absorption from excessive unbound ICG molecules and the self-quenching effect of ICG molecules [45]. Note that the two times difference in the optimal ICG concentration between lasing (0.035–0.04 mM) and regular fluorescence (0.065 mM) is due to the 2 × dilution in blood samples used in our experiment.

4. DISCUSSION AND CONCLUSION

In this work, we demonstrated, to the best of our knowledge, the first "blood laser" using the only FDA approved near-infrared dye, ICG, in human whole blood with the dye concentration within the clinically acceptable range. In addition, we also investigated the ICG lasing behavior in three major serological components (albumins, globulins, and lipoproteins) using the ICG concentration lower than the typical concentration used in *in vitro* studies on cells and excised tumor tissues. In all studies, the pump intensity is orders of magnitude lower than the exposure level that may cause damage to cells or tissues (see Table S1 for summary). Furthermore, we found that it is albumins and lipoproteins that are responsible for ICG lasing and that lipoproteins are far more effective than albumins in achieving ICG lasing.

Our work opens a door to a broad range of clinical and biomedical applications *in vivo* and *in vitro* that provide superior sensitivity and imaging quality to their fluorescence counterparts, such as *in vitro* examination of excised tumor tissues, *in vitro* diagnostics in whole blood (cancer cell detection and monitoring of lipid in blood), *in vivo* tumor margin determination during surgery, preclinical research applications, and single cellular bioanalysis, just to name a few. Together with the recent advancement in optofluidic cellular lasers [21,24–26], lasing in whole blood (which is tissue and generally considered to be closer to actual complex biological samples than cells) represents a critical step toward eventual clinical applications of optofluidic lasers.

As an outlook, below we present a few clinical, preclinical, and biomedical scenarios where the ICG laser may be implemented, and discuss the challenges it faces. (1) Image guided surgery and screening. In this scenario, the ICG is first administered to patients, and then the suspected tumor is removed and examined under a fluorescence microscope. As discussed previously, ICG lasing may help improve differentiation and identification of vital structures in tissues. To implement, a high-Q Fabry–Perot cavity (the Q-factor is as high as 6×10^5 [46], close to that of the OFRR used in the current work) can be employed for *in vitro* biological imaging and spectroscopy due to its planar format. (2) *In vivo* characterization and differentiation of tissues. In this scenario, macroscopic laser cavities such as the Fabry–Perot cavities and ring resonators discussed above may not be applicable. In contrast, the random laser [47,48] and plasmonic laser [49] offer a possible tool to realize lasing at the microscopic and nanoscopic scales. However, it should be noted that those types of laser cavities usually have much lower Q-factors, which may require higher ICG concentrations and pump intensities. Therefore, more work needs to be carried out in the future to develop cavities that are compatible with *in vivo* tissues and have relatively high Q-factors. Meanwhile, new methods that can deliver a higher concentration of ICG, which helps lower the pump intensities required for lasing, while maintaining clinical safety, should also be investigated. One example in this regard is high concentrations of ICG encapsulated in clinically compatible nanoparticle applications recently demonstrated [50,51]. (3) Hyperspectral imaging. It has shown great potential by combining laser spectroscopy with imaging, thereby providing both higher spectral/spatial information and image contrast [15,16,52]. The ICG lasing presented in this article will also lead to the development of novel hyperspectral imaging technologies that complement conventional fluorescence techniques.

5. METHODS

A. Materials

The ICG used in this work was purchased from Sigma-Aldrich (Product #C5753). Other components including HSA

(P8119), LDL (L8292), γ-globulins (G4386), and human serum (H4522) were all purchased from Sigma-Aldrich. BSA and PBS were purchased from R&D systems (Product# 841380, #896009). Human whole blood was purchased from *ZenBio* Inc. (Product# SER-WB10ML), which was collected from healthy volunteers (one male and one female) through Interstate Blood Bank, USA. First, ICG powder was dissolved in DI water to form 2 mM solution, and then it was diluted with DI water to lower concentrations (1 and 0.2 mM). LDL, BSA, HSA, and human serum were originally ordered in solution form, whereas γ-globulins powder was prepared by dissolving it in 0.9% saline. The measured concentrations of LDL, BSA, and HSA in this work were diluted by mixing with 2, 1, or 0.2 mM ICG solutions to obtain the desired compound solutions. For the serum experiments, 200 μL of pure serum was mixed with 50 μL of ICG (1 mM, 0.2 mM) to obtain ICG (0.2 mM, 0.04 mM) compound solutions, respectively. Regarding the whole blood experiments, fresh human blood was first diluted two times with PBS, and then it was added with 0.2 mM ICG to form 0.04 mM compound solution. Other concentrations of ICG used in experiments were prepared similarly. All the prepared samples were allowed to stand for 20 min under room temperature before measuring to ensure the completion of binding reactions of ICG.

B. Fabrication of Optofluidic Ring Resonator

The fabrication of the OFRR has been well documented elsewhere [53]. Briefly, a fused silica capillary preform (Polymicro Technologies TSP700850) was first etched with diluted hydrofluoric acid and then rapidly stretched under CO_2 laser irradiation. The resulting OFRR capillary was slightly bulged with a diameter of 80 μm at the center and of a few micrometers smaller at the two necking points approximately 1 mm apart. The wall thickness of the OFRR was approximately 2–4 μm, and the Q-factor was approximately 10^7 [37,53]. Due to the thin wall, the WGM has a sufficient evanescent field in the core and provides optical feedback for the gain medium flowing inside the capillary to lase.

C. Optical Setup

A typical confocal setup was used to excite the sample and collect emission light from the OFRR (Fig. S9). In this work, a pulsed OPO laser (pulsewidth, 5 ns; repetition rate, 20 Hz) with 660 nm was used as the excitation source to excite a 1 mm portion of the OFRR capillary. The pump intensity was adjusted by a continuously variable neutral density filter. The emission light was collected through the same lens and sent to a spectrometer (Horiba iHR550, spectral resolution ~0.2 nm) for analysis.

Funding. National Institutes of Health (NIH) (NIBIB-1R21EB016783); National Science Foundation (NSF) (ECCS-1607250).

See Supplement 1 for supporting content.

REFERENCES

1. B. E. Schaafsma, J. S. D. Mieog, M. Hutteman, J. R. Van der Vorst, P. J. Kuppen, C. W. Löwik, J. V. Frangioni, C. J. Van de Velde, and A. L. Vahrmeijer, "The clinical use of indocyanine green as a near-infrared fluorescent contrast agent for image-guided oncologic surgery," J. Surg. Oncol. **104**, 323–332 (2011).
2. J. T. Alander, I. Kaartinen, A. Laakso, T. Pätilä, T. Spillmann, V. V. Tuchin, M. Venermo, and P. Välisuo, "A review of indocyanine green fluorescent imaging in surgery," Int. J. Biomed. Imaging **2012**, 940585 (2012).
3. N. Kokudo and T. Ishizawa, "Clinical application of fluorescence imaging of liver cancer using indocyanine green," Liver Cancer **1**, 15–21 (2012).
4. S. L. Troyan, V. Kianzad, S. L. Gibbs-Strauss, S. Gioux, A. Matsui, R. Oketokoun, L. Ngo, A. Khamene, F. Azar, and J. V. Frangioni, "The FLARE intraoperative near-infrared fluorescence imaging system: a first-in-human clinical trial in breast cancer sentinel lymph node mapping," Ann. Surg. Oncol. **16**, 2943–2952 (2009).
5. L. Boni, G. David, A. Mangano, G. Dionigi, S. Rausei, S. Spampatti, E. Cassinotti, and A. Fingerhut, "Clinical applications of indocyanine green (ICG) enhanced fluorescence in laparoscopic surgery," Surg. Endosc. **29**, 2046–2055 (2015).
6. J. Woitzik, P. Horn, P. Vajkoczy, and P. Schmiedek, "Intraoperative control of extracranial-intracranial bypass patency by near-infrared indocyanine green videoangiography," J. Neurosurg. **102**, 692–698 (2005).
7. J. C. Kraft and R. J. Ho, "Interactions of indocyanine green and lipid in enhancing near-infrared fluorescence properties: the basis for near-infrared imaging *in vivo*," Biochemistry **53**, 1275–1283 (2014).
8. C. Vinegoni, I. Botnaru, E. Aikawa, M. A. Calfon, Y. Iwamoto, E. J. Folco, V. Ntziachristos, R. Weissleder, P. Libby, and F. A. Jaffer, "Indocyanine green enables near-infrared fluorescence imaging of lipid-rich, inflamed atherosclerotic plaques," Sci. Transl. Med. **3**, 84ra45 (2011).
9. S. Yoneya, T. Saito, Y. Komatsu, I. Koyama, K. Takahashi, and J. Duvoll-Young, "Binding properties of indocyanine green in human blood," Invest. Ophthalmol. Vis. Sci. **39**, 1286–1290 (1998).
10. C. Zheng, M. Zheng, P. Gong, D. Jia, P. Zhang, B. Shi, Z. Sheng, Y. Ma, and L. Cai, "Indocyanine green-loaded biodegradable tumor targeting nanoprobes for in vitro and in vivo imaging," Biomaterials **33**, 5603–5609 (2012).
11. M. Ogawa, N. Kosaka, P. L. Choyke, and H. Kobayashi, "*In vivo* molecular imaging of cancer with a quenching near-infrared fluorescent probe using conjugates of monoclonal antibodies and indocyanine green," Cancer Res. **69**, 1268–1272 (2009).
12. C. Fang, K. Wang, C. Zeng, C. Chi, W. Shang, J. Ye, Y. Mao, Y. Fan, J. Yang, and N. Xiang, "Illuminating necrosis: from mechanistic exploration to preclinical application using fluorescence molecular imaging with indocyanine green," Sci. Rep. **6**, 21013 (2016).
13. K. Wang, W. Sun, C. T. Richie, B. K. Harvey, E. Betzig, and N. Ji, "Direct wavefront sensing for high-resolution *in vivo* imaging in scattering tissue," Nat. Commun. **6**, 7276 (2015).
14. G. Lu and B. Fei, "Medical hyperspectral imaging: a review," J. Biomed. Opt. **19**, 010901 (2014).
15. R. P. Judy, J. J. Keating, E. M. DeJesus, J. X. Jiang, O. T. Okusanya, S. Nie, D. E. Holt, S. P. Arlauckas, P. S. Low, and E. J. Delikatny, "Quantification of tumor fluorescence during intraoperative optical cancer imaging," Sci. Rep. **5**, 16208 (2015).
16. N. Lue, J. W. Kang, C.-C. Yu, I. Barman, N. C. Dingari, M. S. Feld, R. R. Dasari, and M. Fitzmaurice, "Portable optical fiber probe-based spectroscopic scanner for rapid cancer diagnosis: a new tool for intraoperative margin assessment," PLoS One **7**, e30887 (2012).
17. Y. Sun and X. Fan, "Distinguishing DNA by analog-to-digital-like conversion by using optofluidic lasers," Angew. Chem. Int. Ed. **51**, 1236–1239 (2012).
18. X. Zhang, W. Lee, and X. Fan, "Bio-switchable optofluidic lasers based on DNA Holliday junctions," Lab Chip **12**, 3673–3675 (2012).
19. Q. Chen, X. Zhang, Y. Sun, M. Ritt, S. Sivaramakrishnan, and X. Fan, "Highly sensitive fluorescent protein FRET detection using optofluidic lasers," Lab Chip **13**, 2679–2681 (2013).
20. X. Wu, M. K. Khaing Oo, K. Reddy, Q. Chen, Y. Sun, and X. Fan, "Optofluidic laser for dual-mode sensitive biomolecular detection with a large dynamic range," Nat. Commun. **5**, 3779 (2014).
21. X. Fan and S.-H. Yun, "The potential of optofluidic biolasers," Nat. Methods **11**, 141–147 (2014).
22. M. Aas, Q. Chen, A. Jonáš, A. Kiraz, and X. Fan, "Optofluidic FRET lasers and their applications in novel photonic devices and biochemical sensing," IEEE J. Sel. Top. Quantum Electron. **22**, 1–15 (2016).
23. Y.-C. Chen, Q. Chen, and X. Fan, "Optofluidic chlorophyll lasers," Lab Chip **16**, 2228–2235 (2016).
24. M. C. Gather and S. H. Yun, "Single-cell biological lasers," Nat. Photonics **5**, 406–410 (2011).

25. M. Humar and S. H. Yun, "Intracellular microlasers," Nat. Photonics **9**, 572–576 (2015).
26. Q. Chen, A. Kiraz, and X. Fan, "Optofluidic FRET lasers using aqueous quantum dots as donors," Lab Chip **16**, 353–359 (2016).
27. Q. Chen, M. Ritt, S. Sivaramakrishnan, Y. Sun, and X. Fan, "Optofluidic lasers with a single molecular layer of gain," Lab Chip **14**, 4590–4595 (2014).
28. W. Lee and X. Fan, "Intracavity DNA melting analysis with optofluidic lasers," Anal. Chem. **84**, 9558–9563 (2012).
29. V. Sabapathy, J. Mentam, P. M. Jacob, and S. Kumar, "Noninvasive optical imaging and *in vivo* cell tracking of indocyanine green labeled human stem cells transplanted at superficial or in-depth tissue of SCID mice," Stem Cells Int. **2015**, 606415 (2015).
30. S. Balaiya, V. S. Brar, R. K. Murthy, and K. Chalam, "Effects of indocyanine green on cultured retinal ganglion cells in-vitro," BMC Res. Notes **2**, 236 (2009).
31. T. Yamada, M. Yoshikawa, S. Kanda, Y. Kato, Y. Nakajima, S. Ishizaka, and Y. Tsunoda, "In vitro differentiation of embryonic stem cells into hepatocyte-like cells identified by cellular uptake of indocyanine green," Stem Cells **20**, 146–154 (2002).
32. C. Abels, S. Karrer, W. Bäumler, A. E. Goetz, M. Landthaler, and R. M. Szeimies, "Indocyanine green and laser light for the treatment of AIDS-associated cutaneous Kaposi's sarcoma," Br. J. Cancer **77**, 1021–1024 (1998).
33. D. Holt, A. B. Parthasarathy, O. Okusanya, J. Keating, O. Venegas, C. Deshpande, G. Karakousis, B. Madajewski, A. Durham, and S. Nie, "Intraoperative near-infrared fluorescence imaging and spectroscopy identifies residual tumor cells in wounds," J. Biomed. Opt. **20**, 076002 (2015).
34. R. Matthes, C. P. Cain, D. Courant, D. A. Freund, B. A. Grossman, P. A. Kennedy, D. J. Lund, M. A. Mainster, A. A. Manenkov, W. J. Marshall, R. McCally, B. A. Rockwell, D. H. Sliney, P. A. Smith, B. E. Stuc, S. A. Tell, M. L. Wolbarsht, and G. I. Zheltov, "Revision of guidelines on limits of exposure to laser radiation of wavelengths between 400 nm and 1.4 μm," Health Phys. **79**, 431–440 (2000).
35. M. Y. Berezin, K. Guo, W. Akers, J. Livingston, M. Solomon, H. Lee, K. Liang, A. Agee, and S. Achilefu, "Rational approach to select small peptide molecular probes labeled with fluorescent cyanine dyes for *in vivo* optical imaging," Biochemistry **50**, 2691–2700 (2011).
36. T. Desmettre, J. Devoisselle, and S. Mordon, "Fluorescence properties and metabolic features of indocyanine green (ICG) as related to angiography," Surv. Ophthalmol. **45**, 15–27 (2000).
37. S. Lacey, I. M. White, Y. Sun, S. I. Shopova, J. M. Cupps, P. Zhang, and X. Fan, "Versatile microfluidic lasers based on opto-fluidic ring resonators," Opt. Express **15**, 15523–15530 (2007).
38. B. Jung, V. I. Vullev, and B. Anvari, "Revisiting indocyanine green: effects of serum and physiological temperature on absorption and fluorescence characteristics," IEEE J. Sel. Top. Quantum Electron. **20**, 149–157 (2014).
39. M. Mihara, I. Kisu, H. Hara, T. Iida, T. Yamamoto, J. Araki, Y. Hayashi, H. Moriguchi, M. Narushima, and K. Banno, "Uterus autotransplantation in cynomolgus macaques: intraoperative evaluation of uterine blood flow using indocyanine green," Hum. Reprod. **26**, 3019–3027 (2011).
40. N. Unno, M. Suzuki, N. Yamamoto, K. Inuzuka, D. Sagara, M. Nishiyama, H. Tanaka, and H. Konno, "Indocyanine green fluorescence angiography for intraoperative assessment of blood flow: a feasibility study," Eur. J. Vasc. Endovasc. Surg. **35**, 205–207 (2008).
41. G. R. Cherrick, S. W. Stein, C. M. Leevy, and C. S. Davidson, "Indocyanine green: observations on its physical properties, plasma decay, and hepatic extraction," J. Clin. Invest. **39**, 592–600 (1960).
42. A. Agarwal, *Fundus Fluorescein and Indocyanine Green Angiography: A Textbook and Atlas* (SLACK Incorporated, 2007).
43. S. Lee, M. W. Lee, H. S. Cho, J. W. Song, H. S. Nam, D. J. Oh, K. Park, W.-Y. Oh, H. Yoo, and J. W. Kim, "Fully integrated high-speed intravascular optical coherence tomography/near-infrared fluorescence structural/molecular imaging in vivo using a clinically available near-infrared fluorescence-emitting indocyanine green to detect inflamed lipid-rich atheromata in coronary-sized vessels," Circulation **7**, 560–569 (2014).
44. P. R. van den Biesen, F. H. Jongsma, G. J. Tangelder, and D. W. Slaaf, "Yield of fluorescence from indocyanine green in plasma and flowing blood," Ann. Biomed. Eng. **23**, 475–481 (1995).
45. S. Mordon, J. M. Devoisselle, S. Soulie-Begu, and T. Desmettre, "Indocyanine green: physicochemical factors affecting its fluorescence *in vivo*," Microvasc. Res. **55**, 146–152 (1998).
46. W. Wang, C. Zhou, T. Zhang, J. Chen, S. Liu, and X. Fan, "Optofluidic laser array based on stable high-Q Fabry–Pérot microcavities," Lab Chip **15**, 3862–3869 (2015).
47. R. C. Polson and Z. V. Vardeny, "Random lasing in human tissues," Appl. Phys. Lett. **85**, 1289–1291 (2004).
48. J. Ziegler, M. Djiango, C. Vidal, C. Hrelescu, and T. A. Klar, "Gold nanostars for random lasing enhancement," Opt. Express **23**, 15152–15159 (2015).
49. M. A. Noginov, G. Zhu, A. M. Belgrave, R. Bakker, V. M. Shalaev, E. E. Narimanov, S. Stout, E. Herz, T. Suteewong, and U. Wiesner, "Demonstration of a spaser-based nanolaser," Nature **460**, 1110–1112 (2009).
50. P. Liu, C. Yue, B. Shi, G. Gao, M. Li, B. Wang, Y. Ma, and L. Cai, "Dextran based sensitive theranostic nanoparticles for near-infrared imaging and photothermal therapy *in vitro*," Chem. Commun. **49**, 6143–6145 (2013).
51. J. Zheng, N. Muhanna, R. D. Souza, H. Wada, H. Chan, M. K. Akens, T. Anayama, K. Yasufuku, S. Serra, J. Irish, C. Allen, and D. Jaffray, "A multimodal nano agent for image-guided cancer surgery," Biomaterials **67**, 160–168 (2015).
52. D. Mordant, I. Al-Abboud, G. Muyo, A. Gorman, A. Sallam, P. Ritchie, A. Harvey, and A. McNaught, "Spectral imaging of the retina," Eye **25**, 309–320 (2011).
53. S. I. Shopova, H. Zhu, X. Fan, and P. Zhang, "Optofluidic ring resonator based dye laser," Appl. Phys. Lett. **90**, 221101 (2007).